Available online at www.sciencedirect.com
ScienceDirect
Geochimica et Cosmochimica Acta 75 (2011) 284–296
Geochimica et Cosmochimica Acta
www.elsevier.com/locate/gca

# Effect of pH on calcite growth at constant $a_{Ca^{2+}}/a_{CO_3^{2-}}$ ratio and supersaturation

E. Ruiz-Agudo [a,*], C.V. Putnis [a], C. Rodriguez-Navarro [b], A. Putnis [a]

[a] *Institut für Mineralogie, University of Münster, Corrensstrasse 24, 48149 Münster, Germany*
[b] *Dept. Mineralogía y Petrología, Universidad de Granada, Fuentenueva s/n, 18002 Granada, Spain*

Received 25 June 2010; accepted in revised form 28 September 2010; available online 8 October 2010

**Abstract**

*In situ* Atomic Force Microscopy (AFM) was used to study the growth of calcite at a constant supersaturation ($\Omega = 6.5$) and solution stoichiometry ($a_{Ca^{2+}}/a_{CO_3^{2-}} = 1$) in the pH range 7.5–12. The calcite growth rate decreased with increasing pH in the studied range. The results can be successfully explained by the surface complexation model for calcite growth and by considering the effect of $OH^-$ ions on solute hydration. At pH below 8.5, growth occurs mainly by $CaCO_3^0$ incorporation at $>CaHCO_3^0$ surface sites. $CaCO_3^0$ should be more easily incorporated than free $Ca^{2+}$ ions, as water exchange is usually faster if water molecules in the ion hydration shells are substituted by other ligands, as in $CaCO_3^0$. However, at pH above 9, $Ca^{2+}$ incorporation at $>CaHCO_3^0$ sites also contributes to calcite growth as a result of the increased frequency of water exchange in calcium hydration shells due to the presence of strongly hydrated $OH^-$. This also leads to an increase in the solid–liquid interfacial tension at high pH, which seems to reduce the nucleation rate and increase the average size of crystals precipitated in macroscopic, non-seeded experiments. The reduction of calcite growth rate is a consequence of decreasing surface concentration of active growth sites (i.e., $>CaHCO_3^0$) with increasing pH under our experimental conditions.

Changes in two-dimensional island morphology were observed at high pH (12), possibly due to the stabilization of polar scalenohedral faces by the presence of $OH^-$ ions. This work may help to improve our understanding of the effects of carbonate–solution reactions resulting from potential changes in the pH of the oceans and surface waters in response to variations in atmospheric $CO_2$, as well as in understanding calcite precipitation in highly alkaline environments both natural (e.g., alkali lakes) and artificial (e.g., cement carbonation).


## 1. INTRODUCTION

Reactions between calcite and solution (growth, dissolution and replacement) are critical in a range of both engineering and natural processes such as the removal of heavy metals from the environment by adsorption or coprecipitation on calcite surfaces (Davis et al., 1987; García-Sánchez and Álvarez-Ayuso, 2002), carbon dioxide sequestration (O'Connor et al., 1999; Wolf et al., 2004; Béarat et al., 2006), landscape modeling and evolution (Trenhaile, 1987), the deterioration of building stone (Bell, 1993) and biomineralization (Mann, 2001). This has motivated research resulting in an extensive literature on the growth and the dissolution of calcite (see, for example, the review by Morse et al., 2007). Classical crystal growth theory relates calcite growth rates to the degree of supersaturation. However, the solution composition may also affect the growth rate of carbonate minerals, via the $Ca^{2+}$ to $CO_3^{2-}$ concentration ratio (Nehrke et al., 2007; Perdikouri et al., 2009; Larsen et al., 2010; Stack and Grantham, 2010), ionic strength (Zuddas and Mucci, 1998) or the presence of organic matter (Hoch et al., 2000). The effect of the different parameters that may influence the kinetics of calcite growth must be quantified in isolation.

Calcite precipitation occurs in nature in a wide range of slightly to highly alkaline environments. In alkaline or soda

* Corresponding author. Tel.: +49 (0)251 83 36107; fax: +49 (0)251 83 38397.
*E-mail address:* eruiz_01@uni-muenster.de (E. Ruiz-Agudo).

0016-7037/$ - see front matter © 2010 Elsevier Ltd. All rights reserved.
doi:10.1016/j.gca.2010.09.034

lakes calcite precipitation occurs at high pH (9.3–9.8), supersaturation (SI = 1–1.4) and ionic strength (0.1–1.6) (Kempe and Kazmierczack, 1997). Knowledge of calcite precipitation rates and growth morphologies under these conditions may help in establishing criteria for recognizing saline alkaline lake deposits in the geological record. High pH and calcium concentration are typical of fluids emanating from serpentinized ultramafic rocks in mid-ocean ridges. Calcium carbonate precipitation occurs upon contact of these fluids with seawater, at pH between 9.0 and 9.8, leading to the development of large carbonate chimneys such as those reported in the Lost City vent field (30°N, Mid-Atlantic Ridge) (Kelley et al., 2001). Natural, low temperature hydration and carbonation of mantle peridotites outcrops after contact with near-surface groundwater results in carbonate vein and travertine formation at a pH close to 12 (Kelemen and Matter, 2008). This *in situ* mineral carbonation has been proposed as a potential alternative to *ex situ* methods for capture and storage of anthropogenic $CO_2$ (Kelemen and Matter, 2008; Matter and Kelemen, 2009). The feasibility of this approach for carbon dioxide sequestration requires knowledge and optimization of the reaction kinetics. Furthermore, precipitation of calcium carbonate in marine environments (pH ~ 8.2) is the most important sequestering mechanism for $CO_2$. Changes in the atmospheric $CO_2$ content will affect seawater alkalinity which is linked to global climate. Thus, how pH may influence calcite growth is relevant to improve our understanding of the effects on carbonate–aqueous solution reactions when variations in atmospheric $CO_2$ result in changes in the pH of the oceans and surface waters.

When calcite precipitates from solutions in nature, changes in the pH of the precipitating fluid (as a result of, for example, degassing of atmospheric $CO_2$) result in the modification of the solution speciation and, therefore, of its degree of supersaturation and/or $a_{Ca^{2+}}/a_{CO_3^{2-}}$ ratio (i.e., the calcium to carbonate activity ratio in solution). Furthermore, at fixed supersaturation and lattice ion ratio, pH-sensitive changes in surface speciation may also affect growth kinetics. In order to develop predictive models that account for the influence of all of these parameters in the kinetics of calcite growth, their effects must be quantified in isolation. Most calcite growth studies so far have been performed at a constant pH of ca. 8 or 10. To our knowledge, only two studies (Christoffersen and Christoffersen, 1990; Tai et al., 2006) have specifically considered the effect of pH on calcite growth. In the work by Christoffersen and Christoffersen (1990), the degree of supersaturation with respect to calcite and the $a_{Ca^{2+}}$ to $a_{CO_3^{2-}}$ ratio varied together with the pH, which hindered an unequivocal evaluation of the pH effect on calcite growth kinetics. Tai et al. (2006) explored a limited pH range (8.5–9.5) and, although their work lacks an in-depth interpretation of the observations, they pointed out changes in the solution/crystal interface with variation in pH to explain the observed trend of the growth rate with the pH change.

In the current work, growth rates of single calcite crystals were measured using *in situ* Atomic Force Microscopy as a function of pH, keeping constant both $a_{Ca^{2+}}/a_{CO_3^{2-}}$ ratio and degree of supersaturation at high ionic strength. The results are interpreted in terms of changes in calcite surface speciation with solution pH, using the surface complexation model for calcite growth, and by considering the effect of $OH^-$ ions on solute hydration. Changes in growth morphology at high pH are ascribed to the presence of adsorbed $OH^-$ (as inferred by electrophoretic mobility measurements). Macroscopic, non-seeded experiments were also performed to compare the morphology of the crystals precipitated under these conditions with the morphology of the growth features observed in the AFM experiments.

## 2. METHODOLOGY

### 2.1. Sample and solution preparation

Calcite was cleaved on {1 0 $\bar{1}$ 4} faces of rhombohedral single crystals of optical quality Iceland spar (commercial samples from Chihuahua, Mexico) using a knife blade. The fragments were examined by optical microscopy to ensure that the cleavage surfaces were free from macroscopic steps and small particles. The calcite {1 0 $\bar{1}$ 4} surfaces, ca. 3 × 3 × 1 mm in size, were used as substrates and freshly cleaved prior to each experiment. Calcite growth solutions were prepared by adding calculated volumes of $CaCl_2$ and $NaHCO_3$ from 1 M stock solutions, that were prepared by dissolving reagent grade sodium bicarbonate ($NaHCO_3$, Aldrich) and calcium chloride ($CaCl_2{\cdot}2H_2O$, Aldrich) into doubly deionized water. The precision of added volumes is ±1 μL. The ionic strength (IS) of each growth solution was fixed at 0.1 using reagent grade NaCl (Baker). The pH was adjusted using NaOH or HCl. Neither $CO_2$ nor $Ca(OH)_2$ were used to adjust the pH to ensure that the observed changes in the kinetics and/or mechanisms of calcite growth were due exclusively to changes in the pH, and were not related to changes in solution stoichiometry or supersaturation.

### 2.2. Chemical speciation and supersaturation

The chemical speciation of each solution was determined using the PHREEQC software (Parkhurst and Appelo, 1999) considering the input reservoir and the AFM fluid cell as closed systems (i.e., the amount of $CO_2$ (g) in the system is negligible for the aqueous speciation calculation). Aqueous species considered in the calculation were $HCO_3^-$, $CO_3^{2-}$, $H_2CO_3^0$, $Ca^{2+}$, $CaOH^+$, $CaCO_3^0$, $NaCO_3^-$, $CaHCO_3^+$, $NaHCO_3^0$, $Cl^-$, $Na^+$, and $NaOH^0$. The solution stoichiometry, defined as the ratio of the activities of lattice ions in solution ($a_{Ca^{2+}}/a_{CO_3^{2-}}$), was made equal to 1 by adjusting the amount of $NaHCO_3$ and $CaCl_2$ at the target pH. The supersaturation, $\Omega$, was calculated by $\Omega = IAP/K_{sp}$ where IAP is the ion activity product and $K_{sp}$ the solubility product of calcite ($10^{-8.48}$, phreeqc.dat database) at 25 °C. The solution supersaturation was set at 6.5. This study presents results for pH 7.5–12 using the solution compositions given in Table 1. $Ca^{2+}$ concentrations were measured before and after the AFM runs in selected experiments to estimate the accuracy of the calculated concentrations. With these measurements, the average value of the experimental error associated with the preparation of the solutions was found to be ±0.05 mM.

Table 1
pH, ionic strength (IS), supersaturation ($\Omega$), composition and stoichiometry ($a_{Ca^{2+}}/a_{CO_3^{2-}}$) of the solutions used in each AFM experiment. Measured step advancement ($v_{sum}$, nm s$^{-1}$) and growth ($R$, mol cm$^{-2}$ s$^{-1}$) rates are also given.

| Solution | pH | IS | [$NaHCO_3$] (mM) | [$CaCl_2$] (mM) | [NaCl] (mM) | [NaOH] (mM) | [HCl] (mM) | $\Omega$ | $a_{Ca^{2+}}/a_{CO_3^{2-}}$ | $v_{sum}$ (nm s$^{-1}$) | | R (mol cm$^{-2}$ s$^{-1}$) | |
|---|---|---|---|---|---|---|---|---|---|---|---|---|---|
| | | | | | | | | | | Mean | SD | Mean | SD |
| CCpH0l | 7.50 | 0.13 | 141.60 | 0.68 | 0.000 | 0.00 | 6.00 | 6.5 | 1.00 | 59.64 | 7.81 | 4.20E−09 | 5.5E−10 |
| CCpH02 | 7.75 | 0.10 | 75.65 | 0.54 | 25.35 | 0.00 | 1.49 | 6.5 | 1.00 | 38.29 | 4.80 | 2.70E−09 | 3.4E−10 |
| CCpH03 | 8.00 | 0.10 | 42.30 | 0.48 | 57.70 | 0.00 | 0.00 | 6.5 | 1.00 | 26.90 | 2.17 | 1.89E−09 | 1.5E−10 |
| CCpH04 | 8.25 | 0.10 | 23.95 | 0.45 | 76.05 | 0.00 | 0.00 | 6.5 | 1.00 | 21.71 | 3.05 | 1.53E−09 | 2.2E−10 |
| CCpH05 | 8.50 | 0.10 | 13.72 | 0.43 | 85.65 | 0.63 | 0.00 | 6.5 | 1.00 | 10.14 | 1.34 | 6.28E−10 | 8.1E−11 |
| CCpH06 | 8.75 | 0.10 | 8.00 | 0.42 | 91.32 | 0.68 | 0.00 | 6.5 | 1.00 | 10.14 | 2.65 | 7.14E−10 | 1.1E−10 |
| CCpH07 | 9.00 | 0.10 | 4.79 | 0.42 | 93.53 | 0.69 | 0.00 | 6.5 | 1.00 | 18.54 | 1.96 | 1.18E−09 | 1.1E−10 |
| CCpH08 | 9.25 | 0.10 | 3.00 | 0.41 | 96.17 | 0.71 | 0.00 | 6.5 | 1.00 | 15.51 | 1.97 | 1.02E−09 | 1.1E−10 |
| CCpH09 | 9.50 | 0.10 | 1.98 | 0.41 | 96.30 | 0.72 | 0.00 | 6.5 | 1.00 | 13.81 | 1.52 | 1.03E−09 | 1.4E−10 |
| CCpH10 | 9.75 | 0.10 | 1.41 | 0.41 | 96.83 | 0.76 | 0.00 | 6.5 | 1.00 | 9.52 | 1.92 | 6.85E−10 | 1.17E−10 |
| CCpH11 | 10.00 | 0.10 | 1.09 | 0.41 | 97.09 | 0.82 | 0.00 | 6.5 | 1.00 | 8.89 | 1.75 | 6.38E−10 | 1.26E−10 |
| CCpH12 | 10.25 | 0.10 | 0.91 | 0.41 | 97.18 | 0.93 | 0.00 | 6.5 | 1.00 | 8.30 | 0.87 | 5.84E−10 | 6.1E−11 |

Van Cappellen et al. (1993) proposed a Surface Complexation Model (SCM) for calcite. The SCM was initially derived from the results of macroscopic techniques (surface titration, electrokinetics, and dissolution rate studies), and later confirmed on a microscopic scale using diffuse reflectance infrared spectroscopy (Pokrovsky et al., 2000) and X-ray photoelectron spectroscopy (Fenter et al., 2000). This thermodynamic model for the carbonate/solution interface, postulates the formation of the two primary hydration sites, $>CaOH^0$ and $>CO_3H^0$, having a 1:1 stoichiometry on the (1 0 $\bar{1}$ 4) surface. Note that the notation $>$ is used here to mean surface sites. According to this model, the following complexes are formed from these primary species exposed to the aqueous solution: $>CaOH_2^+$, $>CaO^-$, $>CaHCO_3^0$, $>CaCO_3^-$, $>CO_3Ca^+$ and $>CO_3^-$. The equilibria between these surface groups and aqueous species are described using thermodynamic stability constants. In this study, we used the values provided by Pokrovsky et al. (2000) (Table 2). PHREEQC was used to model the speciation of calcite cleavage surfaces for the aqueous chemical conditions inside the AFM fluid cell in our experiments. A constant thickness of $10^{-8}$ m for the electric double layer was used in the calculations.

### 2.3. ζ potential measurements

ζ potential of calcite particles was determined by electrophoretic mobility measurements at 25 °C, using a Malvern ZetaSizer 2000 instrument. Calcite suspensions were prepared as follows: 0.0136 g of calcite was poured into a volumetric flask containing 50 mL of calcite growth solution to yield a 0.01% volume final solid concentration. The solution compositions used were those employed in AFM experiments. The flasks were gently shaken prior to measurements performed within the first 5 h following preparation of the suspensions. Electrophoretic mobilities can be converted into ζ potential values using the Smoluchowski equation:

$$\zeta = \frac{4\pi\eta}{\varepsilon}\mu \quad (1)$$

where $\eta$ is the viscosity of the solvent, $\varepsilon$ its permittivity and $\mu$ the electrophoretic mobility. The results of electrophoretic measurements are reported as ζ potential values.

### 2.4. AFM *in situ* experiments

Experiments were performed at room temperature in a fluid cell, containing a cleaved calcite crystal, of a Digital Instruments (Veeco Instruments, GmbH) Multimode AFM, working in contact mode. 1.5 mL of growth solutions were injected at intervals of about 1.5 min before each AFM scan, which gave an effective flow rate of approximately 60 mL h$^{-1}$. The flow rates used to measure growth rates were sufficiently high to ensure surface control. As pointed out by Arvidson et al. (2006), this strategy is consistent with many of the published AFM experiments that address both calcite dissolution (e.g., Liang et al., 1996) and growth (e.g., Teng et al., 1998). The experiments were repeated in a Digital Instruments Dimension D-3000 AFM (Veeco Instruments, GmbH) to compare results,

Table 2
Surface complexation reactions and their stability constants at the calcite/solution interface (modified from Pokrovsky et al., 2000).

| Reaction on the surface | Log K (25 °C) |
|---|---|
| $> CO_3H^0 \Rightarrow CO_3^- + H^+$ | −5.1 |
| $> CO_3H^0 + Ca^{2+} \Rightarrow > CO_3Ca^+ + H^+$ | −1.7 |
| $> CaOH^0 \Rightarrow > CaO^- + H^+$ | −12.0 |
| $> CaOH^0 + H^+ \Rightarrow > CaOH_2^+$ | 11.5 |
| $> CaOH^0 + CO_3^{2-} + 2H^+ \Rightarrow > CaHCO_3^0 + H_2O$ | 23.5 |
| $> CaOH^0 + CO_3^{2-} + H^+ \Rightarrow > CaCO_3^- + H_2O$ | 17.1 |

the latter instrument allowing greater possibility to observe a larger scan area as well as to move more freely to other growth sites on the same surface.

Images were continuously taken and the time automatically recorded. AFM images were collected using $Si_3N_4$ tips (Veeco Instruments, tip model NP-S20) with spring constants 0.12 N m$^{-1}$ and 0.58 N m$^{-1}$. Images were analyzed using the NanoScope software (version 5.12b48). The step advancement rate given by $v_{sum}$ (nm s$^{-1}$) $= v_+ + v_-$ (where $v_+$ and $v_-$ are the advancement velocities of obtuse and acute steps, respectively) was calculated as a function of pH by measuring the length increase per unit time along both the [4 8 $\bar{1}$] and [$\bar{4}$ 4 1] directions in sequential images. The scanned area was typically (5 × 5) or (15 × 15) μm (larger for the D-3000). Multiple independent experiments were performed for most of the experimental conditions to ensure reproducibility of observations and measurements (error bars indicate standard deviation of the values measured). By analogy with dissolution rates (Shiraki et al., 2000), growth rates can be calculated from AFM measurements using the equation:

$$R = \left(\frac{v_{sum}}{V_M}\right) \cdot \left(\frac{\Delta h}{\Delta l}\right) \quad (2)$$

where $V_M$ is the molar volume of calcite (36.93 cm$^3$ mol$^{-1}$) and $(\Delta h/\Delta l)$ is equal to the slope of the calcite surface. We will use in our calculations an average value for $(\Delta h/\Delta l)$ of 0.026 ± 0.015, which is pH-independent and determined for calcite by Shiraki et al. (2000).

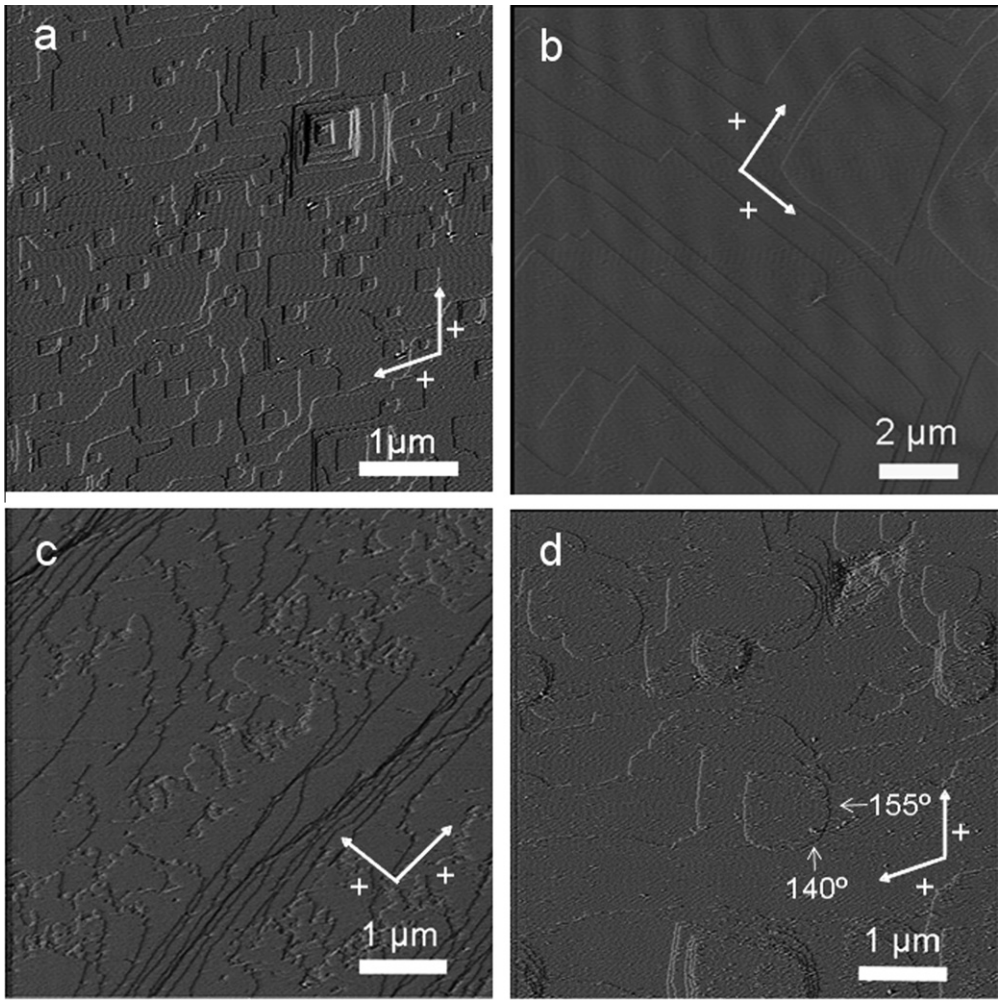


Fig. 1. (a) AFM deflection image of a {1 0 $\bar{1}$ 4} calcite cleavage surface after flowing deionized water over the surface for 2 min. Typical rhombohedral etch pits formed. (b–d) AFM deflection image of calcite growth with solutions with different pH: (b) pH 8.25, (c) pH 8.75, (d) pH 12.

### 2.5. Macroscopic precipitation experiments

Macroscopic non-seeded, spontaneous-precipitation experiments were performed at two different pH values (8.25 and 12) at constant $a_{Ca^{2+}}/a_{CO_3^{2-}} = 1$ and $\Omega = 19.1$. Similar experiments performed at $\Omega = 6.5$ (i.e., the supersaturation ratio in AFM seeded experiments) failed to produce any measurable precipitate even after 1 month, therefore a higher $\Omega$ was selected. The ionic strength (IS) of each growth solution was fixed at 0.1 using reagent grade NaCl (Baker). Solutions were prepared in 100 mL glass flasks by mixing equal volumes of $NaHCO_3$ and $CaCl_2$ aqueous solutions. After 2 weeks, solutions were centrifuged and the solid was dried in an oven (60 °C), carbon coated and analyzed with a JEOL 6300F field emission scanning electron microscope (FESEM).

## 3. RESULTS AND DISCUSSION

### 3.1. Morphology of growth features: stabilization of polar faces by background ions

Calcite growth has been rigorously investigated by Atomic Force Microscopy. The atomic steps on the crystal surfaces reflect its rhombohedral symmetry, with two steps intersecting the $\{1\,0\,\bar{1}\,4\}$ cleavage plane at an acute angle ($[\bar{4}\,4\,1]_-$ and $[4\,8\,\bar{1}]_-$) and two steps intersecting at an obtuse angle ($[\bar{4}\,4\,1]_+$ and $[4\,8\,\bar{1}]_+$). The two obtuse steps are related through a c-glide, as are also the two acute steps. No symmetry operation relates the obtuse steps to the acute steps, i.e., the direction of advancement of opposite steps is not equivalent. This non-equivalence of growth steps determines the growth rate (obtuse steps spread faster than acute steps) (Hillner et al., 1992).

Prior to growth, doubly deionised water (resistivity $> 18\ m\Omega\ cm^{-1}$) was passed over the calcite specimen to clean the surface and to promote the dissolution of surface heterogeneities. Fig. 1a shows a representative image of the calcite surface that has been partly dissolved in water, exhibiting the typical rhombohedral etch pits described elsewhere (see, for example, Arvidson et al., 2006 and references therein). Calcite growth was initiated immediately after injecting the growth solution into the fluid cell. Closure of the dissolution pits, which retain their initial rhombohedral morphology, was first observed and further growth proceeded by the advancement of monomolecular (~3 Å) steps. Under the conditions of our experiments, steps mainly originated from islands generated by two-dimensional surface nucleation (Fig. 1b). Changes in solution pH did not result in significant changes in the observed 2D-island nucleation density. At pH ~ 8.5 where the minimum growth rate was observed, both the pre-existing etch pits as well as the growing step edges became jagged or irregular (Fig. 1c). This may be due to difficulties in incorporating building units into the crystal structure at this pH.

Increasing the pH to 12 led to the nucleation of 2D-islands with rounded $[\bar{4}\,4\,1]_+/[4\,8\,\bar{1}]_+$ corners (Fig. 1d). Note that the step and island morphologies on a growing mineral surface observed using AFM typically have an exact correspondence with the macroscopic form of the crystal (e.g., Kowacz and Putnis, 2008). In fact, similar morphology changes were observed in crystals precipitated in macroscopic non-seeded experiments (Fig. 2). This change in morphology can be interpreted as the result of the overdevelopment of $\{2\,1\,\bar{3}\,1\}$ faces, which was simulated using SHAPE software (www.shapesoftware.com). As can be seen in Fig. 3, the intersection of the overdeveloped $\{2\,1\,\bar{3}\,1\}$ form with the cleavage rhombohedron can result in a rounding of the +/+ corner. The angles calculated for $\{2\,1\,\bar{3}\,1\}$ and $\{1\,0\,\bar{1}\,4\}$ intersection are in agreement with those measured in the AFM images.

Note that when indexing calcite planes, confusion can arise due to the use of four different axial systems, each of which results in a different set of Miller–Bravais indices for a given plane (Hazen, 2004). We use the so-called hexagonal "structural unit-cell" ($a = 5$ Å; $c = 17$ Å) in this paper, in which the Miller indices for the cleavage face are

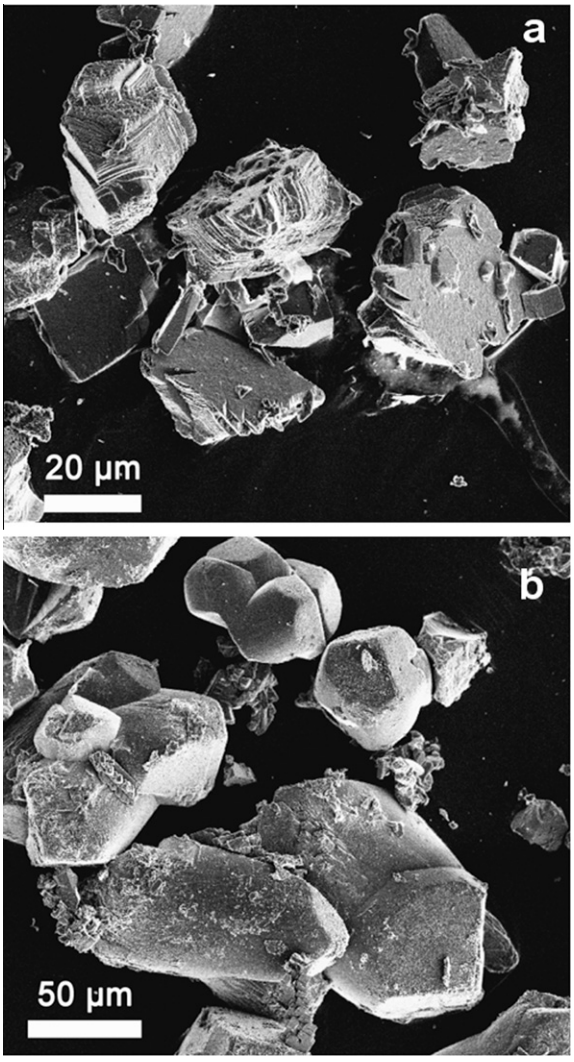


Fig. 2. SEM images of calcite crystals precipitated from solution ($\Omega = 19.1$, $a_{Ca^{2+}}/a_{CO_3^{2-}} = 1$ and IS = 0.1—NaCl) at (a) pH 8.25 and (b) pH 12. Note that the morphology observed in (b) is in good agreement with that simulated using SHAPE software, shown in Fig. 3.

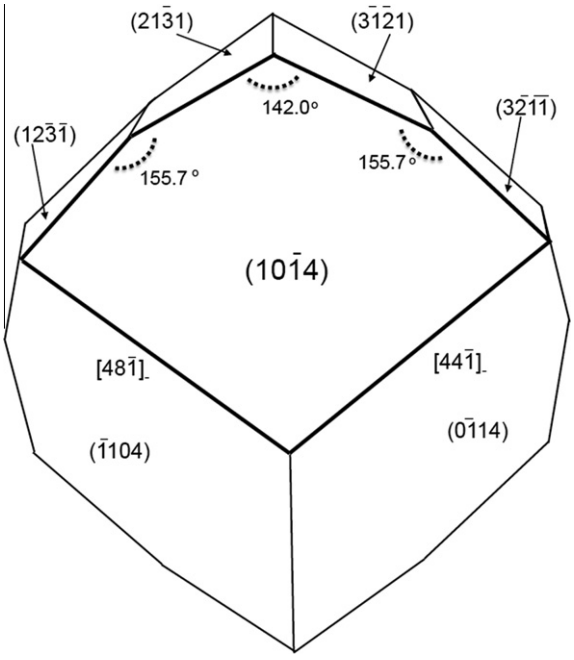


Fig. 3. Morphology simulation of calcite growth islands with overdevelopment of the {2 1 $\bar{3}$ 1} form using SHAPE software. The +/+ corner appears rounded due to the intersection of (2 1 $\bar{3}$ 1), (3 $\bar{2}$ $\bar{2}$ 1), (1 2 $\bar{3}$ $\bar{1}$) and (3 $\bar{2}$ $\bar{1}$ $\bar{1}$) with the (1 0 $\bar{1}$ 4) plane.

(1 0 $\bar{1}$ 4) and (2 1 $\bar{3}$ 4) for the scalenohedral form (Hazen, 2004). In this setting, the {2 1 $\bar{3}$ 1} becomes an elongated scalenohedron.

In contrast to the {1 0 $\bar{1}$ 4} planes, the {2 1 $\bar{3}$ 1} planes are non-stoichiometric and exhibit a (slight) dipole moment (Fig. 4). Surfaces having a repeat unit with a net dipole moment (as a result of non-stoichiometric outcropping of atoms on this face) are known as polar and are not stable under normal growth conditions (i.e., nucleation from pure, stoichiometric solutions). However, scalenohedral forms are frequently observed at high pH (see, for example, the work by García-Carmona et al., 2003a,b) or under conditions of high $a_{Ca^{2+}}/a_{CO_3^{2-}}$ ratios (Lahan, 1978). Stabilization of polar surfaces can be achieved by neutralizing their dipole moment. Introducing vacancies in the outer layers of the crystal will change the density of ions in such layers and may result in the quenching of the dipole moment. The same effect can be achieved by surface reconstruction. However, these changes and thus the resulting surfaces are often of high energy, which grow fast and do not typically appear in the growth form (Duffy and Harding, 2004).

There is an alternative mechanism for the stabilization of such polar faces that consists of adsorbing charged ions onto the crystal surface from solution. This is occasionally achieved by the adsorption of charged, typically organic molecules, which at the growth pH show ionized functional groups. However, in the absence of these "additives", ions present in the original solution may also neutralize such a dipole moment. Hydroxyl ions, which are abundant species at pH 12, can play such a role in stabilizing polar faces. The presence of adsorbed $OH^-$ at high pH can be inferred from the surface potential ($\Phi_0$) calculations and $\zeta$ potential measurements of calcite in the conditions of our growth experiments.

In the Stern model, $\Phi_0$ of a crystal is related to the activity of the potential-determining ions. Cicerone et al. (1992) showed that the constituent lattice ions are the only potential-determining ions for calcite. $\Phi_0$ can be calculated outside the equilibrium using a general form of the Nernst equation (Donnet et al., 2009):

$$\Phi_0 = \frac{2.303 \cdot RT}{4F}[(p\mathrm{Ca}_{\mathrm{pzc}} - p\mathrm{Ca}) - (p\mathrm{CO}_{3\mathrm{pzc}} - p\mathrm{CO}_3)] \quad (3)$$

where $R$ is the gas constant, $T$ is the temperature, $F$ is the Faraday constant and the subscript pzc stands for the potential at zero charge ($\Phi_0 = 0$). We used $pCa_{\mathrm{pzc}} = 3.97$ and $pCO_{3\mathrm{pzc}} = 4.51$ (25 °C, Donnet et al., 2009). Since $p$Ca and $p\mathrm{CO}_3$ are equal and constant in our experiments (3.83), the surface charge remains constant and equal to −7.98 mV. Surface and $\zeta$ potential experimentally measured differ due to the position of the shear plane where $\zeta$ potential is measured (i.e., hydrodynamic conditions of the solution) and accumulation of ions in the Stern layer, and both can be correlated using the equation (Donnet et al., 2009):

$$\xi \cong \Psi \cdot \Phi_0 + C_0 \quad (4)$$

where $\Psi$ reflects the position of the shear plane and depends only on the measuring method, while $C_0$ corrects for the adsorption of non-specific (i.e., non-potential-determining)

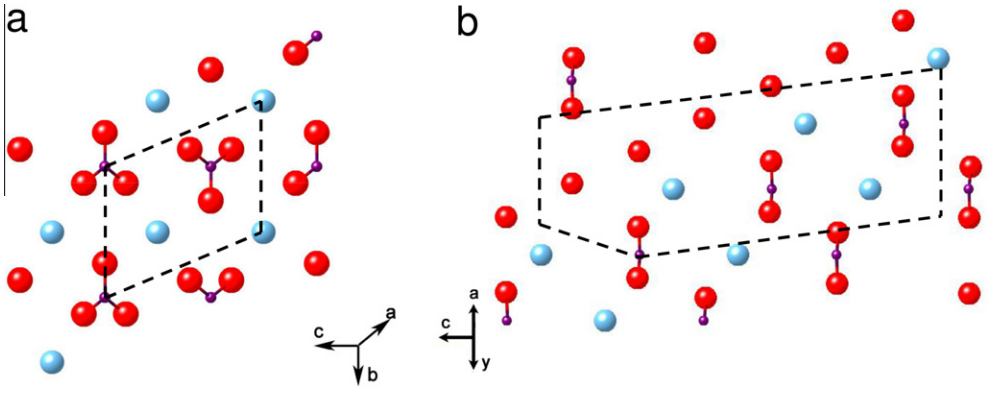


Fig. 4. Atomistic slab models of (a) {1 0 $\bar{1}$ 4} and (b) {2 1 $\bar{3}$ 1} surfaces. The dashed line represents the intersection with the unit cell.

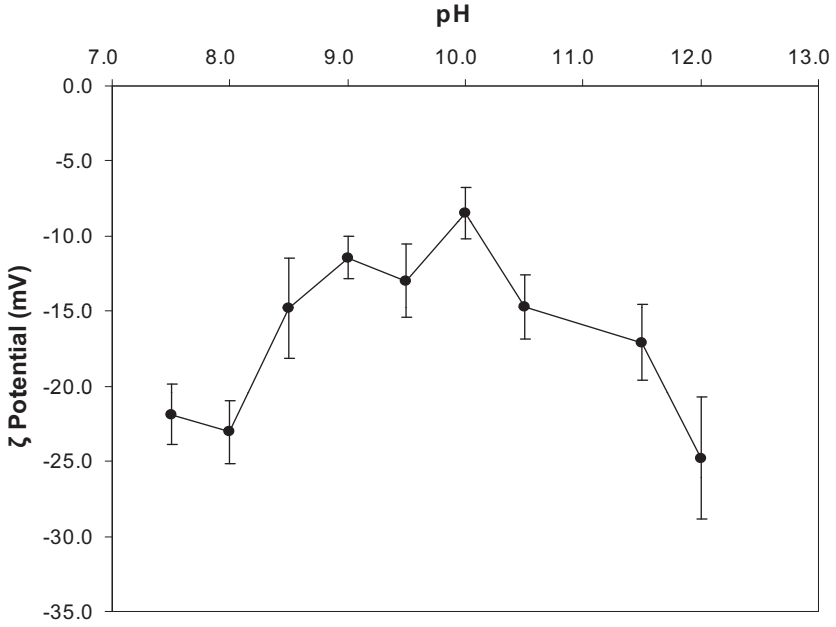


Fig. 5. Measured ζ potential values as a function of pH for calcite powder in contact with solutions used in AFM experiments.

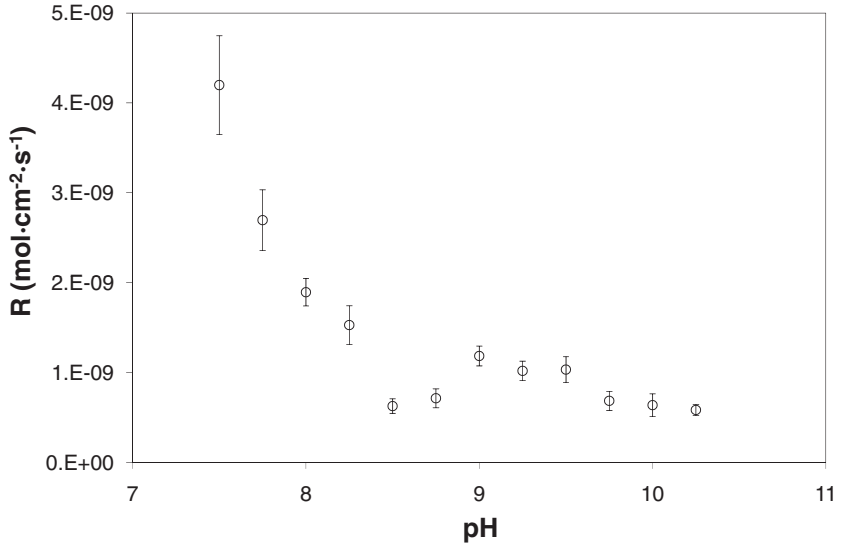


Fig. 6. AFM measured growth rate ($R$, mol cm$^{-2}$ s$^{-1}$) vs. pH of the solution at $a_{Ca^{2+}}/a_{CO_3^{2-}} = 1$, $\Omega = 6.36$ and IS = 0.1 (NaCl). Error bars denote standard deviations.

ions in the Stern layer. The ζ potential variations as a function of pH are plotted in Fig. 5. Since both $\Psi$ (measurement conditions) and $\Phi_0$ are constant, this variation arises from changes in $C_0$ due to adsorption of non-specific ions in the Stern layer. In our case, $HCO_3^-$ (at pH < 10) and $OH^-$ (at pH > 10) are possibly responsible for such differences.

We hypothesize that at high pH the small dipole moment of scalenohedral faces may be neutralized, due to the presence of adsorbed $OH^-$ ions. This results in {2 1 $\bar{3}$ 1} stabilization during calcite growth. As already mentioned, this is reflected in changes in the morphology of 2D-islands nucleated on calcite cleavage surfaces during growth at pH 12. Perdikouri et al. (2009) also observed rounded +/+ corners at high and low $Ca/CO_3$ ratios. In this case, the adsorption of the excess $Ca^{2+}$ or $CO_3^{2-}$ may compensate the dipolar moment. Development of scalenohedral faces has been reported when calcite is obtained during carbonation of $Ca(OH)_2$ solutions (García-Carmona et al., 2003a,b). In that case, however, the effect of $OH^-$ and $a_{Ca^{2+}}/a_{CO_3^{2-}}$ ratio cannot be isolated. A similar effect is observed when calcite nucleation and growth occurs in the presence of organic electrolytes (see the work by Duffy and Harding, 2004 and

Table 3
Speciation of the aqueous solutions used in each AFM experiment modeled using PHREEQC. The species $H_2CO_3$ and $CO_2$(aq) are summed up as $H_2CO_3$.

| Solution | $HCO_3^-$ | $CO_3^{2-}$ | $H_2CO_3$ | $Ca^{2+}$ | $CaOH^+$ | $CaCO_3$ | $NaCO_3^-$ | $CaHCO_3^+$ | $NaHCO_3$ | $Cl^-$ | $Na^+$ | NaOH |
|---|---|---|---|---|---|---|---|---|---|---|---|---|
| CCpH01 | 9.86E−02 | 1.46E−04 | 7.04E−03 | 1.46E−04 | 7.64E−10 | 3.59E−05 | 2.82E−04 | 1.84E−04 | 5.75E−03 | 5.46E−03 | 1.04E−01 | 2.16E−08 |
| CCpH02 | 5.54E−02 | 1.46E−04 | 2.22E−03 | 1.46E−04 | 1.36E−09 | 3.59E−05 | 2.10E−04 | 1.04E−04 | 2.40E−03 | 2.14E−02 | 7.70E−02 | 2.85E−08 |
| CCpH03 | 3.12E−02 | 1.46E−04 | 7.03E−04 | 1.46E−04 | 2.42E−09 | 3.59E−05 | 2.10E−04 | 5.82E−05 | 1.35E−03 | 4.49E−02 | 7.71E−02 | 5.07E−08 |
| CCpH04 | 1.75E−02 | 1.46E−04 | 2.23E−04 | 1.46E−04 | 4.30E−09 | 3.59E−05 | 2.11E−04 | 3.27E−05 | 7.64E−04 | 5.84E−02 | 7.75E−02 | 9.07E−08 |
| CCpH05 | 9.87E−03 | 1.46E−04 | 7.04E−05 | 1.46E−04 | 7.65E−09 | 3.59E−05 | 2.12E−04 | 1.84E−05 | 4.31E−04 | 6.61E−02 | 7.77E−02 | 1.62E−07 |
| CCpH06 | 5.55E−03 | 1.46E−04 | 2.23E−05 | 1.46E−04 | 1.36E−08 | 3.59E−05 | 2.12E−04 | 1.04E−05 | 2.43E−04 | 7.04E−02 | 7.78E−02 | 2.88E−07 |
| CCpH07 | 3.12E−03 | 1.46E−04 | 7.04E−06 | 1.46E−04 | 2.42E−08 | 3.59E−05 | 2.10E−04 | 5.82E−06 | 1.35E−04 | 7.21E−02 | 7.72E−02 | 5.08E−07 |
| CCpH08 | 1.76E−03 | 1.46E−04 | 2.23E−06 | 1.46E−04 | 4.30E−08 | 3.59E−05 | 2.12E−04 | 3.27E−06 | 7.68E−05 | 7.41E−02 | 7.79E−02 | 9.12E−07 |
| CCpH09 | 9.86E−04 | 1.46E−04 | 7.04E−07 | 1.46E−04 | 7.65E−08 | 3.59E−05 | 2.10E−04 | 1.84E−06 | 4.29E−05 | 7.42E−02 | 7.73E−02 | 1.61E−06 |
| CCpH10 | 5.55E−04 | 1.46E−04 | 2.23E−07 | 1.46E−04 | 1.36E−07 | 3.59E−05 | 2.11E−04 | 1.04E−06 | 2.41E−05 | 7.46E−02 | 7.73E−02 | 2.86E−06 |
| CCpH11 | 3.12E−04 | 1.46E−04 | 7.03E−08 | 1.46E−04 | 2.42E−07 | 3.59E−05 | 2.10E−04 | 5.82E−07 | 1.35E−05 | 7.48E−02 | 7.73E−02 | 5.09E−06 |
| CCpH12 | 1.75E−04 | 1.46E−04 | 2.22E−08 | 1.46E−04 | 4.30E−07 | 3.59E−05 | 2.10E−04 | 3.27E−07 | 7.62E−06 | 7.49E−02 | 7.73E−02 | 9.05E−06 |

references therein). In this case, both (0 1 $\bar{1}$ 2) and (0 0 0 1) faces are frequently reported, although they are highly polar and not stable during growth from pure solutions. Stabilization of polar faces due to the presence of electrolytes has been also observed during calcite dissolution in the presence of $F^-$ (Ruiz-Agudo et al., 2010) or during barite dissolution in the presence of different background electrolytes (Kowacz and Putnis, 2008). Lea et al. (2001) and Arvidson et al. (2003) also observed rounding of +/+ step intersections during calcite dissolution. Nevertheless, this observation most probably has a different origin; the pH in these experiments was considerably lower (pH 8.8) than in our experiments where the rounding was observed (pH 12), and the solutions contained a much higher carbonate concentration; this effect, as stated by the authors, is most likely due to $HCO_3^-/CO_3^{2-}$ adsorption on +/+ corners of the etch pits.

Another interesting effect of the presence of abundant $OH^-$ was a clear increase in crystal size observed in the macroscopic precipitation experiments at pH 12 compared to pH 8.25. In both cases a homogeneous particle size distribution was observed, with a mean crystal size of ca. 90 and 30 μm, respectively (Fig. 2). It should be considered that the higher the nucleation rate, the smaller the resulting particle size. At a constant driving force for crystallization, differences in the nucleation rate will arise from differences in the kinetic barrier for nucleation and/or solid–liquid interfacial tension. Both are related to the frequency of water exchange around the building units of the crystal (Kowacz et al., 2010). Higher frequencies will result in higher values of interfacial tension (which lead to a decreased nucleation rate and increased particle size) but also in a lower kinetic barrier for ion desolvation (which should increase the nucleation rate and, as a consequence, reduce the particle size) (Kowacz et al., 2010).

The hydroxyl ion, $OH^-$, has a structure-maker character (i.e., it is an ion with a high charge density that causes strong electrostatic ordering of water molecules in its first solvation shell) and is strongly hydrated in solution (Marcus, 1994). Its presence will therefore augment the competition for water of hydration between the H-bonded network of water and the solute ions, resulting in an increase in the frequency of water exchange around the latter and thus in the interfacial tension. In our case, this effect seems to prevail over the decrease in the kinetic barrier for nucleation, as higher particle sizes are observed at pH 12.

### 3.2. Kinetics of calcite growth: surface speciation and changes in calcium hydration

Table 1 summarizes the conditions (pH, solution composition, solution stoichiometry and supersaturation) and the results of each AFM flow-through experiment. Because the inlet solutions were prepared immediately before use, atmospheric $CO_2$ is considered to be negligible. The growth ($R$, mol cm$^{-2}$ s$^{-1}$) and etch pit spreading ($v_{sum}$, nm s$^{-1}$) rate values are reported in Table 1, and growth rates are plotted against pH in Fig. 6. As an indication of the validity and reproducibility of the kinetic data obtained in this study, they can be directly compared, for example, to those

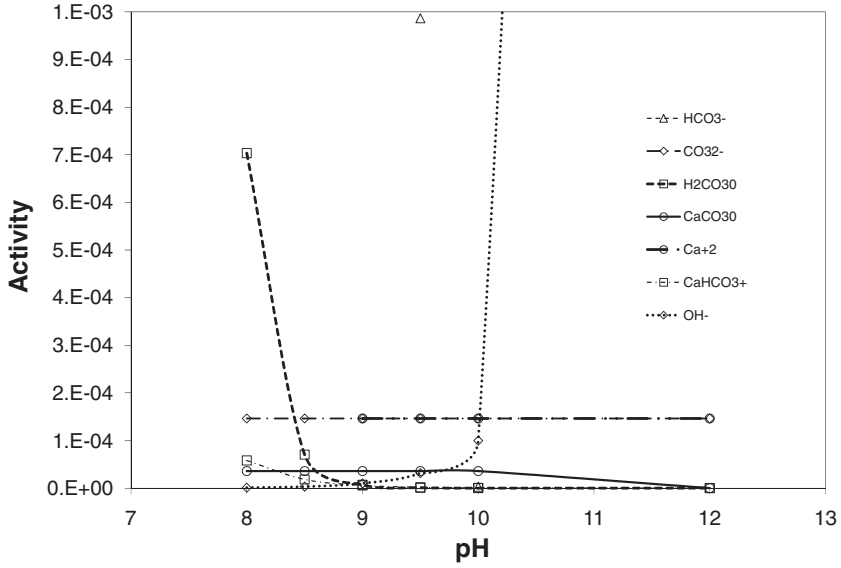


Fig. 7. PHREEQC modeling of the aqueous solution composition in AFM experiments as a function of pH. The species $H_2CO_3$ and $CO_2$(aq) are summed up as $H_2CO_3$.

Table 4
Speciation of a calcite cleavage surface in contact with the solutions used in AFM experiments modeled using PHREEQC.

| Solution | $>CO_3H^0$ | | | $>CaOH^0$ | | | | |
|---|---|---|---|---|---|---|---|---|
| | $[>CO_3Ca^+]$ (mol $m^{-2}$) | $[>CO_3^-]$ (mol $m^{-2}$) | $[>CO_3H]$ (mol $m^{-2}$) | $[>CaCO_3^-]$ (mol $m^{-2}$) | $[>CaOH_2^+]$ (mol $m^{-2}$) | $[>CaHCO_3]$ (mol $m^{-2}$) | [>CaOH] (mol $m^{-2}$) | $[>CaO^-]$ (mol $m^{-2}$) |
| CCpH01 | 1.16E−04 | 4.19E−05 | 4.59E−07 | 1.05E−04 | 3.04E−05 | 2.30E−05 | 4.93E−10 | 5.67E−15 |
| CCpH02 | 1.18E−04 | 4.06E−05 | 2.56E−07 | 1.11E−04 | 3.37E−05 | 1.40E−05 | 9.51E−10 | 1.90E−14 |
| CCpH03 | 1.19E−04 | 3.99E−05 | 1.43E−07 | 1.15E−04 | 3.57E−05 | 8.22E−06 | 1.77E−09 | 6.22E−14 |
| CCpH04 | 1.19E−04 | 3.94E−05 | 8.01E−08 | 1.17E−04 | 3.70E−05 | 4.75E−06 | 3.23E−09 | 2.00E−13 |
| CCpH05 | 1.20E−04 | 3.92E−05 | 4.50E−08 | 1.18E−04 | 3.77E−05 | 2.71E−06 | 5.84E−09 | 6.40E−13 |
| CCpH06 | 1.20E−04 | 3.90E−05 | 2.53E−08 | 1.19E−04 | 3.82E−05 | 1.54E−06 | 1.05E−08 | 2.04E−12 |
| CCpH07 | 1.20E−04 | 3.89E−05 | 1.42E−08 | 1.20E−04 | 3.84E−05 | 8.69E−07 | 1.87E−08 | 6.47E−12 |
| CCpH08 | 1.20E−04 | 3.89E−05 | 7.98E−09 | 1.20E−04 | 3.85E−05 | 4.90E−07 | 3.34E−08 | 2.05E−11 |
| CCpH09 | 1.20E−04 | 3.89E−05 | 4.49E−09 | 1.20E−04 | 3.86E−05 | 2.76E−07 | 5.95E−08 | 6.49E−11 |
| CCpH10 | 1.20E−04 | 3.90E−05 | 2.53E−08 | 1.20E−04 | 3.86E−05 | 1.55E−07 | 1.06E−07 | 2.05E−10 |
| CCpH11 | 1.20E−04 | 3.88E−05 | 1.42E−09 | 1.20E−04 | 3.86E−05 | 8.73E−08 | 1.88E−07 | 6.50E−10 |
| CCpH12 | 1.20E−04 | 3.89E−05 | 7.97E−10 | 1.20E−04 | 3.86E−05 | 4.91E−08 | 3.34E−07 | 2.05E−09 |

reported by Perdikouri et al. (2009). These authors reported values of growth rate between 7.5 and 11 nm $s^{-1}$ at $\Omega = 6.5$, pH 10.356 and $a_{Ca^{2+}}/a_{CO_3^{2-}} \sim 1$, well in agreement with the rate observed in our experiments at pH 10.25 ($v_{sum} = 8.30 \pm 0.87$). $R$ values decrease with increasing pH in the studied range (7.5–10), reaching a minimum at pH 8.5. Between pH 8.5 and 9.0, there is a slight increase in the growth rate, which smoothly decreases again upon further increase of the pH up to 10.

Calculated solution and surface speciation data are reported in Table 3, Fig. 7, and Table 4, Fig. 8, respectively. Since the results of surface speciation modeling are sensitive to the exact solution composition, they were calculated for our experimental conditions using data from Table 1. The surface speciation predicted by the surface complexation model varied only over the pH range 7–8.5, and remained mostly unchanged from pH 8.5 to 10 (only the surface concentration of $>CaHCO_3^0$ changed). The dominant calcium surface species from pH 7 to 12 is $>CaCO_3^-$. $>CaOH_2^+$ is also important, and $>CaHCO_3^0$ concentration is significant in the 7–8 pH range. In the speciation of superficial carbonate groups, the $>CO_3Ca^+$ species dominates over the entire pH range. However, as shown by Fenter et al. (2000), the log $K$ value proposed by Pokrovsky et al. (2000) for the formation of such a complex is an overestimate, thus the predicted activity of $>CO_3Ca^+$ surface species in our experiments could be smaller.

The observed dependence of calcite growth kinetics on solution pH can be explained considering the mechanistic model for the kinetics of carbonate crystal growth, initially proposed by Sternbeck (1997) for rhodochrosite and later applied to calcite by Nilsson and Sternbeck (1999). This model attempts to explain the kinetics of carbonate reactivity based on the mechanisms of the reactions occurring at

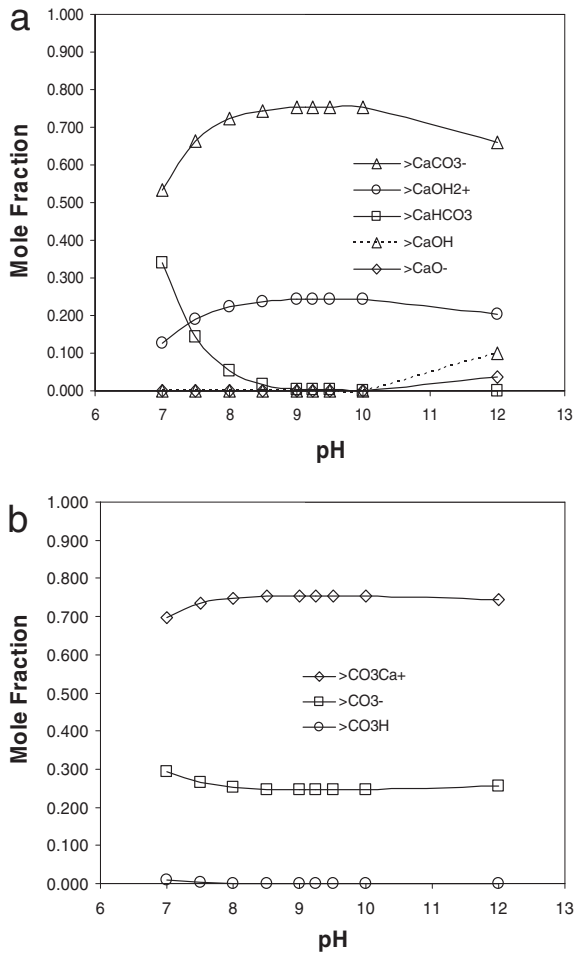


Fig. 8. PHREEQC modeling of the calcite surface speciation in contact with solutions used for AFM experiments as a function of pH: (a) metal sites and (b) carbonate sites.

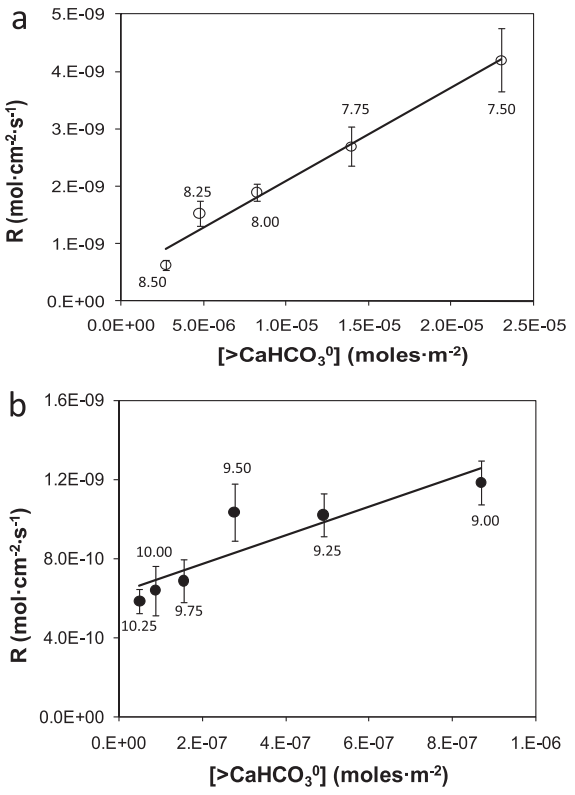


Fig. 9. AFM measured growth rates ($R$, mol cm$^{-2}$ s$^{-1}$) vs. [>$CaHCO_3^0$] (mol m$^{-2}$) on a calcite surface as a function of pH: (a) $7.5 < pH < 8.5$ and (b) $9 < pH < 10$. Individual pH values are indicated close to the data points.

the mineral aqueous solution interface during growth. It assumes that the process of incorporation of dissolved species at mineral surfaces is similar to ligand exchange in solution, thus implying that the reaction pathways involved in ligand exchange can be used to describe reactions leading to crystal growth. According to this model, crystal growth is governed by adsorption of lattice ions on the dehydrated surface species >$CO_3Ca^+$, >$CO_3^-$, >$CaHCO_3^0$, and >$CaCO_3^-$. Calcite growth requires equivalent adsorption on carbonate and calcium sites and therefore adsorption on those sites that are in the minority should be the rate-determining step. Under the conditions of the present study, >$CaHCO_3^0$ is the dehydrated species with the smaller surface concentration. Adsorption on >$CaHCO_3^0$ is therefore likely to be the rate-determining step. The nearly continuous decrease in $R$ over the studied pH range is thus due to the reduction in the population of active surface sites >$CaHCO_3^0$. Regarding the aqueous species that are incorporated at this surface site, it should be noted that calcite growth requires cation dehydration before incorporation into the crystal lattice. Since in strong ion pairs such as the $CaCO_3^0$ ion, the cation is partially dehydrated, it is plausible to assume that $CaCO_3^0$ could integrate faster than $Ca^{2+}$ into the crystal lattice. Thus, the main adsorbing species in this model would be $CaCO_3^0$.

According to Nilsson and Sternbeck (1999), calcite crystal growth can be described by the following reaction:

$$> CaHCO_3^0 + CaCO_3^0 \leftrightarrow > CaHCO_3^0 + 6H_2O \quad \text{(Reaction1)}$$

However, as these authors pointed out, in addition to $CaCO_3^0$, $Ca^{2+}$ may adsorb and dehydrate on the calcite surface and therefore it may be incorporated at the mineral surface. With increasing pH, dehydration of $Ca^{2+}$ will be kinetically favored and its incorporation into the $CaCO_3$ structure would play a more important role in calcite growth under such conditions. As stated above, the presence of hydroxyl ions will result in an increase in the frequency of water exchange around the solute ions. Thus increasing pH will facilitate $Ca^{2+}$ dehydration and its surface adsorption and subsequent incorporation into the calcite lattice. A similar behavior has been observed for KCl (Mohameed and Ulrich, 1996). Under the conditions of our experiments, only the reaction involving $Ca^{2+}$ adsorption at >$CaHCO_3^0$ gave a good fit to experimental data, so we suggest that $Ca^{2+}$ is incorporated also at >$CaHCO_3^0$ surface sites. Therefore, with increasing pH, the following reaction will increasingly contribute to calcite crystal growth:

$$> CaHCO_3^0 + Ca^{2+} \leftrightarrow > CO_3Ca^+ + H^+ + 8H_2O \quad \text{(Reaction2)}$$

The forward reaction describes crystal growth and the backward describes dissolution by hydrolysis. The rate of calcite crystal growth (i.e., forward Reactions (1) and (2)) can be thus described as:

$$R = k_1 \cdot (CaCO_3^0) \cdot [> CaHCO_3^0] + k_2 \cdot (Ca^{2+}) \cdot [> CaHCO_3^0] \quad (5)$$

where $k_1$ and $k_2$ are rate constants for forward Reactions (1) and (2), respectively, activity in solution is denoted ( ), and the density of a surface complex on the mineral surface is denoted [ ] (mol $m^{-2}$).

We consider two different regimes: one at pH < 8.5, where the main contribution to calcite growth is due to $CaCO_3^0$ incorporation at $>CaHCO_3^0$ sites; and another at pH > 9 where the dehydration of $Ca^{2+}$ induced by the increased presence of $OH^-$ allows $Ca^{2+}$ incorporation at the mineral surface. At this pH, although $CaCO_3^0$ may also be incorporated, the higher activity in solution of $Ca^{2+}$ compared to $CaCO_3^0$ (see Table 3 and Fig. 6) makes its incorporation into the calcite structure the main contribution to the overall growth rate. For 8.5 < pH < 9, there is a transitional regime where both reactions play a role. In this transitional regime, the growth rate increases as a consequence of the increasing contribution of $Ca^{2+}$ species to growth as a result of its more favorable dehydration due to the presence of $OH^-$ ions.

Growth rates in these two regimes can be approximated using the following equations:

$$\text{pH} < 8.5 \qquad R \approx k_1 \cdot (CaCO_3^0) \cdot [> CaHCO_3^0] \quad (6)$$

$$\text{pH} > 9 \qquad R \approx k_2 \cdot (Ca^{2+}) \cdot [> CaHCO_3^0] \quad (7)$$

A similar approach was used by Duckworth and Martin (2003) for the case of rhodochrosite dissolution. They proposed a step-site surface complexation model, which reconciles both surface complexation models and morphological and geometric models, to quantitatively relate growth rates to the surface chemical speciation of steps. Because $k_1$, $k_2$, $(CaCO_3^0)$ and $(Ca^{2+})$ are constant, the average step velocity is proportional to the surface concentration of $>CaHCO_3^0$ sites. This approach to the effect of pH on calcite growth can be tested by plotting $R$ vs. $[>CaHCO_3^0]$. Straight lines having slopes of $k_1 \cdot (CaCO_3^0)$ and $k_2 \cdot (Ca^{2+})$ are obtained, as seen in Fig. 9a and b, respectively. The correlation coefficient, $r$, equals 0.976 and 0.808 and the slopes of the plots are 1.63 and 7.25 $s^{-1}$ for the pH < 8.5 and pH > 9 regimes, respectively.

Using the calculated ion activities in solution, the rate constants $k_1$ and $k_2$ were found to equal $1.63 \times 10^8$ and $1.78 \times 10^8$ $h^{-1}$, respectively. Both $Ca^{2+}$ and $CaCO_3^0$ are adsorbed on the same surface complex, $>CaHCO_3^0$, which enables direct comparison of the rate constants. The values of $k_1$ and $k_2$ are approximately equal which indicates that $Ca^{2+}$ and $CaCO_3^0$ are incorporated at similar rates to $>CaHCO_3^0$. The reaction of a ligand with a hydrated metal ion weakens the bonds to the hydrating water and increases the rate of exchange of water molecules between the inner sphere and bulk solution (Piana et al., 2006). Thus, $CaCO_3^0$ should be more easily incorporated than free $Ca^{2+}$ ions, because dehydration of the adsorbing species must precede crystal growth. However, as we have already stated, at high pH the increased concentration of hydroxyl ions augments the competition for water of hydration between the H-bonded network of water and the calcium ions. This results in an increase in the frequency of water exchange around the latter, thus facilitating its incorporation into the calcite lattice. Furthermore, the $k_1$ value is close to that found by Nilsson and Sternbeck (1999) for the incorporation of $CaCO_3^0$ to $>CaHCO_3^0$ sites ($k = 3.13 \times 10^8$ $h^{-1}$), which further supports the validity of our approach. These authors also found a value of $1.35 \times 10^7$ $h^{-1}$ for the incorporation of $Ca^{2+}$ to $>CaCO_3^-$, which is one order of magnitude lower than that estimated in this study for $Ca^{2+}$ incorporation to $>CaHCO_3^0$. Although these values cannot be directly compared as they refer to incorporation to different surface species, the difference observed is expected as their experiments were performed in the pH range 7.60–8.84, where $Ca^{2+}$ incorporation to any surface species will be hampered due to the strong hydration of the calcium ion.

## 4. CONCLUSIONS

The observed changes in the measured calcite growth rate as a function of pH (at constant solution stoichiometry and supersaturation) are fully consistent with the mechanistic model based on the surface complexation model proposed by Nilsson and Sternbeck (1999). Under the conditions of our experiments, adsorption at the surface species $>CaHCO_3^0$ is probably the rate limiting step. Both $Ca^{2+}$ and $CaCO_3^0$ are incorporated at this surface site from supersaturated solutions. At low pH, $Ca^{2+}$ is strongly hydrated and thus its incorporation is kinetically hampered. $CaCO_3^0$ incorporation is favored as the formation of ion pairs weakens the bonds between the ion and the hydrating water, thus increasing the frequency of water exchange between the hydration shell of calcium and the bulk solution.

With increasing pH, the presence of $OH^-$ may increase the frequency of water exchange around the calcium ion, thus facilitating its incorporation into the calcite structure. $CaCO_3^0$ (at pH < 8.5) and $Ca^{2+}$ (at pH > 9) are incorporated at similar rates to $>CaHCO_3^0$. However, the decrease in surface concentration of active growth sites (i.e., $>CaHCO_3^0$) with increasing pH results in the observed decrease in calcite growth rates with increasing pH.

Other interesting effects of the higher concentration of $OH^-$ are the modification of the calcite 2D-island morphology, apparently due to its adsorption at and stabilization of $(2\,1\,\bar{3}\,1)$ faces, and the decrease in crystal size, possibly related to the increase in solid–liquid interfacial tension caused by the modification of frequency of water exchange around the calcium ion.

## ACKNOWLEDGMENTS

This work has been financially supported by the EU Initial Training Network Delta-Min (Mechanisms of Mineral Replacement Reactions) Grant PITN-GA-2008-215360. Experimental facilities are supported by the Deutsche Forschungsgemeinschaft (DFG). Financial support has also been provided by the research

group NRM-179 (Junta de Andalucía, Spain). We thank A. Delgado from the Applied Physics Department, Universidad de Granada, for his assistance during ζ potential measurements. We thank the editor, George Helz and three anonymous reviewers for the constructive comments which have helped to improve this paper.

## REFERENCES

Arvidson R. S., Ertan I. E., Amonette J. E. and Luttge A. (2003) Variations in calcite dissolution rates: a fundamental problem? *Geochim. Cosmochim. Acta* **67**, 1623–1624.

Arvidson R. S., Collier M., Davis K. J., Vinson M. D., Amonette J. E. and Luttge A. (2006) Magnesium inhibition of calcite dissolution kinetics. *Geochim. Cosmochim. Acta* **70**, 583–594.

Béarat H., McKelvy M. J., Chizmeshya A. V., Gormley D., Nunez R., Carpenter R. W., Squires K. and Wolf G. H. (2006) Carbon sequestration via aqueous olivine mineral carbonation: role of passivating layer formation. *Environ. Sci. Technol.* **40**, 4802–4808.

Bell F. G. (1993) Durability of carbonate rock as building stone with comments on its preservation. *Environ. Geol.* **21**, 187–200.

Christoffersen J. and Christoffersen M. R. (1990) Kinetics of spiral growth of calcite crystals and determination of the absolute rate constant. *J. Cryst. Growth* **100**, 203–211.

Cicerone D. S., Regazzoni A. E. and Blesa M. A. (1992) Electrokinetic properties of the calcite/water interface in the presence of magnesium and organic matter. *J. Colloid Interf. Sci.* **154**, 423–433.

Davis J. A., Fuller C. and Cook A. D. (1987) A model for trace metal sorption processes at the calcite surface: adsorption of $Cd^{2+}$ and subsequent solid solution formation. *Geochim. Cosmochim. Acta* **51**, 1477–1490.

Donnet M., Bowen P. and Lemaitre J. (2009) A thermodynamic solution model for calcium carbonate: towards an understanding of multi-equilibria precipitation pathways. *J. Colloid Interf. Sci.* **340**, 218–224.

Duckworth O. W. and Martin S. T. (2003) Connections between surface complexation and geometric models of mineral dissolution investigated for rhodochrosite. *Geochim. Cosmochim. Acta* **67**, 1787–1801.

Duffy D. M. and Harding J. H. (2004) Growth of polar crystal surfaces on ionized organic substrates. *Langmuir* **20**, 7637–7642.

Fenter P., Geissbühler P., Dimasi E., Srajer G., Sorensen L. B. and Sturchio N. C. (2000) Surface speciation of calcite observed in situ by high-resolution X-ray reflectivity. *Geochim. Cosmochim. Acta* **64**, 1221–1228.

García-Carmona J., Gomez Morales J. and Rodriguez Clemente R. (2003a) Rhombohedral–scalenohedral calcite transition produced by adjusting the solution electrical conductivity in the system $Ca(OH)_2$–$CO_2$–$H_2O$. *J. Colloid Interf. Sci.* **261**, 434–440.

García-Carmona J., Gomez Morales J. and Rodriguez Clemente R. (2003b) Morphological control of precipitated calcite obtained by adjusting the electrical conductivity in the $Ca(OH)_2$–$H_2O$–$CO_2$ system. *J. Cryst. Growth* **249**, 561–571.

García-Sánchez A. and Álvarez-Ayuso E. (2002) Sorption of Zn, Cd and C on calcite. Application to purification of industrial wastewaters. *Miner. Eng.* **15**, 539–547.

Hazen R. M. (2004) Chiral crystal faces of common rock-forming minerals. In *Progress in Biological Chirality* (eds. G. Palyi, C. Zucchi and L. Caglioti). Elsevier, Oxford, pp. 137–151.

Hillner P. E., Gratz A. J., Manne S. and Hansma P. K. (1992) Atomic-scale imaging of calcite growth and dissolution in real time. *Geology* **20**, 359–362.

Hoch A. R., Reddy M. M. and Aiken G. R. (2000) Calcite crystal growth inhibition by humic substances with emphasis on hydrophobic acids from the Florida Everglades. *Geochim. Cosmochim. Acta* **64**, 61–72.

Kelemen P. B. and Matter J. (2008) In situ carbonation of peridotite for $CO_2$ storage. *Proc. Natl. Acad. Sci. USA* **105**, 17295–17300.

Kelley D. S., Karson J. A., Blackman D. K., Früh-Green G. L., Butterfield D. A., Lilley M. D., Olson E. J., Schrenk M. O., Roe K. K., Lebon G. T. and Rivizzigno P. (2001) An off-axis hydrothermal vent field near the Mid-Atlantic Ridge at 30°N. *Nature* **412**, 145–149.

Kempe S. and Kazmierczack J. (1997) A terrestrial model for an alkaline martian hydrosphere. *Planet. Space Sci.* **11**, 1493–1499.

Kowacz M. and Putnis A. (2008) The effect of specific background electrolytes on water structure and solute hydration: consequences for crystal dissolution and growth. *Geochim. Cosmochim. Acta* **72**, 4476–4487.

Kowacz M., Prieto M. and Putnis A. (2010) Kinetics of nucleation in ionic solutions: electrostatics and hydration forces. *Geochim. Cosmochim. Acta* **74**, 469–481.

Lahan R. W. (1978) A chemical model for calcite crystal growth and morphology. *J. Sed. Petrol.* **48**, 337–344.

Larsen K., Bechgaard K. and Stipp S. L. S. (2010) The effect of the $Ca^{2+}$ to $CO_3^{2-}$ activity ratio on spiral growth at the calcite $\{1\,0\,\bar{1}\,4\}$ surface. *Geochim. Cosmochim. Acta* **74**, 2099–2109.

Lea A. S., Amonette J. E., Baer D. R., Liang Y. and Colton N. G. (2001) Microscopic effects of carbonate, manganese and strontium ions on calcite dissolution. *Geochim. Cosmochim. Acta* **65**, 369–379.

Liang Y., Baer D. R., McCoy J. M., Amonette J. E. and LaFemina J. P. (1996) Dissolution kinetics at the calcite–water interface. *Geochim. Cosmochim. Acta* **60**, 4883–4887.

Mann S. (2001) *Biomineralization: Principles and Concepts in Bioinorganic Materials Chemistry*. Oxford University Press, Oxford.

Marcus Y. (1994) Viscosity B-coefficients, structural entropies and heat capacities, and the effects of ions on the structure of water. *J. Sol. Chem.* **23**, 831–848.

Matter J. M. and Kelemen P. B. (2009) Permanent storage of carbon dioxide in geological reservoirs by mineral carbonation. *Nat. Geosci.* **2**, 837–841.

Mohameed H. A. and Ulrich J. (1996) Influence of the pH-value on the growth and dissolution rate of potassium chloride. *Cryst. Res. Technol.* **31**, 27–31.

Morse J. W., Arvidson R. S. and Lüttge A. (2007) Calcium carbonate formation and dissolution. *Chem. Rev.* **107**, 342–381.

Nehrke G., Reichart G. J., Van Cappellen P., Meile C. and Bijma J. (2007) Dependence of calcite growth rate and Sr partitioning on solution stoichiometry: non-Kossel crystal growth. *Geochim. Cosmochim. Acta* **71**, 2240–2249.

Nilsson O. and Sternbeck J. (1999) A mechanistic model for calcite crystal growth using surface speciation. *Geochim. Cosmochim. Acta* **63**, 217–225.

O'Connor W. K., Dahlin D. C., Ochs T. L. and Turner P. C. (1999) *Process for Carbon Dioxide Sequestration by Direct Mineral Carbonation*. U.S. Dept. of Energy, Office of Assistant General Counsel for Patents, Chicago, IL, Record of Invention.

Parkhurst D. L. and Appelo C. A. J. (1999) *Users Guide to PHREEQC (version 2)—A Computer Program for Speciation, Batch Reaction, One-Dimensional Transport, and Inverse Geochemical Calculations*. U.S. Geological Survey Water-Resources Investigation Report 99-4259, 312p.

Perdikouri C., Putnis C. V., Kasioptas A. and Putnis A. (2009) An atomic force microscopy study of the growth of a calcite surface as a function of calcium/total carbonate concentration ratio in solution at constant supersaturation. *Cryst. Growth Des.* **9**, 4344–4350.

Piana S., Jones F. and Gale J. D. (2006) Assisted desolvation as a key kinetic step for crystal growth. *J. Am. Chem. Soc.* **128**, 13568–13574.

Pokrovsky O. S., Mielczarski J. A., Barres O. and Schott J. (2000) Surface speciation models of calcite and dolomite/aqueous solution interfaces and their spectroscopic evaluation. *Langmuir* **16**, 2677–2688.

Ruiz-Agudo E., Kowacz M., Putnis C. V. and Putnis A. (2010) The role of background electrolytes on the kinetics and mechanism of calcite dissolution. *Geochim. Cosmochim. Acta* **74**, 1256–1267.

Shiraki R., Rock P. A. and Casey W. H. (2000) Dissolution kinetics of calcite in 0.1 M NaCl solution at room temperature: an atomic force microscopic (AFM) study. *Aquat. Geochem.* **6**, 87–108.

Stack A. G. and Grantham M. C. (2010) Growth rate of calcite steps as a function of aqueous calcium-to-carbonate ratio: independent attachment and detachment of calcium and carbonate ions. *Cryst. Growth Des.* **10**, 1409–1413.

Sternbeck J. (1997) Kinetics of rhodochrosite crystal growth at 25 °C: the role of surface speciation. *Geochim. Cosmochim. Acta* **61**, 785–793.

Tai C. Y., Chang M.-C., Wu C.-K. and Linet Y.-C. (2006) Interpretation of calcite growth data using the two-step crystal growth model. *Chem. Eng. Sci.* **61**, 5346–5354.

Teng H. H., Dove P. M., Orme C. and De Yoreo J. J. (1998) Thermodynamics of calcite growth: baseline for understanding biomineral formation. *Science* **282**, 724.

Trenhaile A. S. (1987) *The Geomorphology of Rock Coasts*. Oxford University Press, Oxford.

Van Cappellen P., Charlet L., Stumm W. and Wersin P. (1993) A surface complexation model of the carbonate mineral–aqueous solution interface. *Geochim. Cosmochim. Acta* **57**, 3505–3518.

Wolf G. H., Chizmeshya A. V., Diefenbacher J. and McKelvy M. J. E. (2004) In situ observation of $CO_2$ sequestration reactions using a novel microreaction system. *Environ. Sci. Technol.* **38**, 932–936.

Zuddas P. and Mucci A. (1998) Kinetics of calcite precipitation from seawater: II. The influence of the ionic strength. *Geochim. Cosmochim. Acta* **62**, 757–766.

*Associate editor:* George R. Helz